DIGITAL ACCESS TO SCHOLARSHIP AT HARVARD
DASH.HARVARD.EDU

HARVARD LIBRARY
Office for Scholarly Communication

Strategies for Reducing Respiratory Motion Artifacts in Renal Perfusion Imaging With Arterial Spin Labeling

Citation
Robson, Philip M., Ananth J. Madhuranthakam, Weiying Dai, Ivan Pedrosa, Neil M. Rofsky, David Alsop. "Strategies for Reducing Respiratory Motion Artifacts in Renal Perfusion Imaging With Arterial Spin Labeling." Magnetic Resonance in Medicine 61, no. 6 (2009): 1374-1387. DOI: 10.1002/mrm.21960

Published Version
doi:10.1002/mrm.21960

Permanent link
https://nrs.harvard.edu/URN-3:HUL.INSTREPOS:37372562

Terms of Use
This article was downloaded from Harvard University's DASH repository, and is made available under the terms and conditions applicable to Other Posted Material, as set forth at http://nrs.harvard.edu/urn-3:HUL.InstRepos:dash.current.terms-of-use#LAA

Share Your Story

The Harvard community has made this article openly available.
Please share how this access benefits you. Submit a story .

Accessibility

NIH Public Access
Author Manuscript
Magn Reson Med. Author manuscript; available in PMC 2010 September 27.

Published in final edited form as:
Magn Reson Med. 2009 June ; 61(6): 1374–1387. doi:10.1002/mrm.21960.

Strategies for Reducing Respiratory Motion Artifacts in Renal Perfusion Imaging with Arterial Spin Labeling

Philip M. Robson[1], **Ananth J. Madhuranthakam**[2], **Weiying Dai**[1], **Ivan Pedrosa**[1], **Neil M. Rofsky**[1], and **David C. Alsop**[1]

[1]Department of Radiology, Beth Israel Deaconess Medical Center, Boston, MA and Harvard Medical School, Boston, MA

[2]Global MR Applied Science Laboratory, GE Healthcare, Boston, MA

Abstract

Arterial Spin Labeling (ASL) perfusion measurements may have many applications outside the brain. In the abdomen, severe image-artifacts can arise from motions between acquisitions of multiple signal averages in ASL, even with single-shot image-acquisition. Background suppression and respiratory motion synchronization techniques can be used to ameliorate these artifacts. Two separate in-vivo studies of renal perfusion imaging using pulsed-continuous ASL were performed. The first study assessed various combinations of background suppression and breathing strategies. The second investigated the retrospective sorting of images acquired during free breathing based on respiratory position. Quantitative assessments of the test-retest repeatability of perfusion measurements and the image quality scored by two radiologists were made. Image quality was most significantly improved by using background suppression schemes and controlled breathing when compared to other combinations without background suppression or with free breathing, assessed by test-retests (5% level, *F*-test), and by radiologists' scores (5% level, Mann-Whitney U-test). Under free breathing, retrospectively sorting images based on respiratory position showed significant improvement. Both radiologists found 100% of the images had preferable image sharpness after sorting. High quality renal perfusion measurements with reduced respiratory motion artifacts have been demonstrated using ASL when appropriate background suppression and breathing strategies are applied.

Keywords

Renal Perfusion; Pulsed-Continuous Arterial Spin Labeling; pCASL; Background Suppression; Motion Artifacts; Respiratory Motion; Physiological Motion

Introduction

Arterial Spin Labeling (ASL) (1–4) is a well-established method for imaging and quantitatively measuring tissue-perfusion in the brain (5–10). Applications of ASL in the body to date have shown promise (11–16). However, ASL perfusion imaging in the body is not currently widely used. ASL works by selectively magnetically labeling arterial water, and thus, provides a technique for measuring renal blood flow with MRI without the need to administer gadolinium-based contrast agents. This is of great potential importance when evaluating patients with renal insufficiency for whom the risk of gadolinium-based contrast

Correspondence to Dr. Philip Robson, Dept. of Radiology, Ansin 242, Beth Israel Deaconess Medical Center, 330 Brookline Avenue, Boston, MA 02215, 617 667-0273, fax 617-667-7917, probson@bidmc.harvard.edu.

NIH-PA Author Manuscript
NIH-PA Author Manuscript
NIH-PA Author Manuscript

NIH-PA Author Manuscript

NIH-PA Author Manuscript

NIH-PA Author Manuscript

administration may be undesirable (17). Quantification of renal blood flow with ASL may also be simpler than with dynamic contrast methods, for which nonlinearity of signal intensity, vascular permeability, and the movement of contrast between cortical and medullary compartments complicates measurement.

By selectively magnetically labeling inflowing blood, ASL can replace the signal-enhancement of inflowing blood induced with administration of an exogenous substance. The difference in signal between images acquired with a magnetic label applied (label) and without (control) reveals the perfusion of the tissue. The difference in the signal for label- and control images is typically a few percent of the tissue signal and, therefore, ASL difference images can suffer from the influence of image noise. Typically, many repetitions of the ASL measurement are averaged together to increase signal-to-noise ratio (SNR). This requirement extends the time for acquisition of a perfusion image to some minutes making the whole experiment prone to motion corruption during the acquisition time. From this perspective, the application of ASL in the abdomen is particularly challenging. Physiological effects such as peristalsis of the bowel and pulsations of surrounding organs can be problematic. Furthermore, care must be taken to deal with the gross displacements of the abdomen during the respiratory cycle.

Motion artifacts in ASL of the abdomen can be severe, but several techniques can be used to reduce or eliminate them. Motion between the acquisitions of different *k*-space data points can yield non-local artifacts on images. These artifacts can be largely eliminated by the use of fast, single-shot imaging techniques such as echo-planar imaging or single-shot rapid acquisition with relaxation enhancement (RARE). Such non-local artifacts may still be a concern in volumetric imaging sequences and they may also benefit from the artifact reduction approaches employed here, however they are not further addressed in this work. Motion artifacts still arise in single-shot ASL imaging, however, because multiple images must be averaged and subtracted to produce an ASL image with a favorable SNR. Even with imaging sequences where motion is inconspicuous on anatomical images, motion artifacts may be a few percent of the image signal and thus can be comparable to the perfusion signal upon subtraction. Fortunately, different strategies for greatly reducing subtraction errors in ASL are available, including background suppression and respiratory motion synchronization techniques.

Angiographic (18,19) and ASL applications (20–22) have made use of background suppression schemes employing multiple inversion pulses to suppress signals from background tissues, which contribute to physiologic noise and lead to image artifacts. Though background suppression itself is not a motion-correction technique, it helps to reduce motion artifact that appears in the subtraction of misregistered label and control images to a tolerable level because this subtraction error is proportional to the background signal. Extending the concept of signal nullification in an inversion-recovery preparation, application of multiple inversion pulses prior to imaging can effectively nullify signals from tissues with a range of longitudinal relaxivities. Reductions of background signal greater than 50 fold (22) can readily be achieved, with a corresponding reduction of motion-related subtraction errors. Even a single inversion, as performed in FAIR studies of abdominal ASL (12,13,15), can be very helpful at reducing background signal and subtraction errors.

A variety of techniques for synchronizing scanning to respiratory position have been developed for abdominal and thoracic MR imaging. In clinical abdominal imaging, gross respiratory motions are typically managed by either acquiring data within a breath-hold, or by gating acquisition to some point in the respiratory cycle. Breath-held acquisitions in healthy volunteers generally provide adequate cessation of abdominal motion allowing acquisition of largely artifact-free images but in certain patient populations the success of

NIH-PA Author Manuscript

NIH-PA Author Manuscript

NIH-PA Author Manuscript

breath-holding will be limited. Where single acquisitions are not possible and multiple interleaves of data are acquired, images can become corrupted by motion-induced errors in the signal due to the longer time delays between the acquisitions of neighboring parts of *k*-space. Prospective triggering using respiratory bellows is a successful strategy for limiting such errors (23,24). However, ASL techniques comprise a time-sensitive labeling and in-flow period of several seconds prior to data acquisition. If triggering is performed at the beginning of labeling, then motion may occur before image acquisition. If triggering is performed for image acquisition, then the time of labeling can vary widely and severe subtraction errors will occur if RF pulses are applied to the tissue of interest at the beginning of labeling, as in FAIR or background suppressed studies. Other prospective techniques such as navigator echo triggering (25,26) are also prone to the problem of irregular respiratory motions between trigger and data acquisition during the magnetization preparation period. Patterned breathing strategies have also been suggested (13,27) to ameliorate image degradation from data acquired during free breathing. Previous studies of ASL in the abdomen used a variety of breathing strategies, including breath-hold (11,13–15), free breathing (12,15), and patterned breathing (13). Navigator techniques have previously been used (16), and background suppression inversion pulses (14) have also been employed.

Here, we studied background suppression schemes in combination with various breathing strategies that could lead to improved performance of quantitative abdominal ASL perfusion imaging. Qualitative image appearance, test-retest reproducibility, and region-of-interest noise standard deviations that include contributions from motion related noise were used as measures of successful motion artifact reduction. Given that a clinical population may poorly tolerate patterned breathing strategies, free-breathing acquisitions were also considered.

Methods

Two separate in-vivo studies in healthy volunteers were performed. The first assessed various combinations of background suppression and breathing strategies. The second investigated retrospectively sorting images acquired during free breathing based on respiratory position. All studies were performed with written informed consent of subjects after obtaining approval for the study from the hospital Institutional Review Board. All experiments were performed on a 1.5-Tesla Excite-HDx imager (GE Healthcare, Waukesha, WI) using the product 8-channel body receiver-array for reception, the body-coil for transmission and the product single-shot fast spin echo (SSFSE) sequence, modified with pulsed-continuous ASL (pCASL) preparation (28), for image acquisition.

STUDY 1: Background Suppression and Breathing Strategies

In a cohort of four healthy volunteers (3 female, 1 male, mean age 38, range 19–62), combinations of background suppression schemes and breathing strategies were tested. The entire exam was repeated 1 week later on each subject to assess test-retest reliability. After a scout image and standard multi-slice axial and coronal partial-Fourier SSFSE images had been acquired for localization, the perfusion measurements were made with several different combinations of respiratory synchronization and background suppression types. Specifics of the respiratory and background suppression strategies are provided in subsections of the methods below. The following combinations of respiratory synchronization and background suppression type were evaluated in each subject: A) Breathing voluntarily timed to synchronize with the image acquisition (timed breathing) with each of: i) heavy background suppression, ii) moderate suppression, and iii) no suppression; B) A series of five breath-held acquisitions comprising three reference scans (proton density and two T1 weighted images used for flow quantification, see “Reference Image Acquisition” section below) followed by four multiples of four ASL measurements with: i) heavy background

NIH-PA Author Manuscript

NIH-PA Author Manuscript

NIH-PA Author Manuscript

suppression, and ii) moderate suppression; C) Free breathing with: i) heavy background suppression, and ii) moderate suppression; D) Timed breathing with heavy background suppression as in (Ai) repeated. E) A 2D phase contrast renal angiography sequence was performed to measure total renal flow to provide an independent indication of renal perfusion. Respiratory bellows were worn by each subject allowing confirmation of cooperation with breathing instructions during the experiment. The same order of experiments was followed for all subjects. Each breathing pattern was sufficiently different from each other that systematic habituation was not considered likely. Observation of the subjects' breathing via the trace of respiratory bellows indicated that this was justified, showing that all subjects followed breathing instructions well with no pattern to their occasional "missed breaths".

For both timed and free breathing, 16 spin-labeled label-control pairs were acquired. For the multiple breath-hold strategy, only 8 label-control pairs were acquired due to the additional time required between breath-held acquisitions. Timed and free breathing perfusion measurements lasted for 3.5 minutes, while breath-held measurements lasted approximately 10 minutes in total comprising 1.9 minutes of imaging over five breath-holds with breaks between for breathing. The whole imaging session duration was approximately one hour.

Each subject was imaged twice, a week apart, to assess repeatability of perfusion measurements. At retest the imaging plane was carefully cross-referenced to a saved image from the previous session. At retest, the measurements in (B) were performed before those in (A) to prevent habituation arising from the subjects' familiarity with the previous session. At retest, measurements in (D) were omitted.

STUDY 2: Retrospective Respiratory Sorting

In a separate cohort of four healthy volunteers (4 female, mean age 48, range 29–57), ASL perfusion measurement during free breathing was performed with recording of respiratory bellows signal to optimize retrospective motion reduction strategies. Heavy background suppression was used for all images in this part of the study. ASL measurements were performed as follows: F) Under free breathing, a block of ASL measurements with three reference images (also acquired while free-breathing) and 12 ASL label-control pairs was repeated four times in close succession for a combined scan time of 10.8 minutes. This acquisition gave a selection of perfusion label-control pairs and reference images over the entire range of respiratory positions for evaluation of post-processing methods. G) For comparison, the timed breathing strategy ((Ai) above) was also performed with three reference images and 16 ASL label-control pairs. Measurements (F) and (G) were then repeated to obtain a test-retest measurement. Finally, one extra series, (H) with three reference scans and 16 ASL label-control pairs, was run in which the subject was asked to breathe heavily throughout to produce large abdominal displacements during data acquisition. The order of imaging was the same for all subjects.

Respiratory bellows position was recorded immediately prior to each image acquisition and was used to sort images and eliminate those which were significantly out-of-position for both the reference scans and ASL images in the measurements in (F). Four acceptance criteria were investigated. A set of references images comprising one of each type were selected that were: i) the first set acquired, ii) the saturation and inversion recovery reference images closest to end-expiration, iii) the images closest to the median bellows position of all the ASL images, and iv) the group of images with the minimum sum of squared differences between bellows positions. For the ASL images: i) an acceptance window of ±25% of all the ASL images was placed on the position of the first reference image, ii) images with bellows position below the median value were used, i.e. those images closest to end-expiration, iii) images between the 25th and 75th percentiles were used, and iv) an acceptance window of

NIH-PA Author Manuscript

NIH-PA Author Manuscript

NIH-PA Author Manuscript

±25% of all the ASL images was placed on the position of the mean value of the three reference images that were closest together.

ACQUISITION PARAMETERS

Imaging Sequences—The ASL imaging slice was positioned to include a cross-section of both kidneys. An oblique-coronal image orientation was used, centered on the midline of the body at the level of the renal arteries. Care was taken to position the slice such that the entireties of both kidneys were inferior to the labeling plane of the ASL magnetization preparation (see the "Arterial Spin Labeling" section). The imaging slice was not moved during the session ensuring exact registration between imaging locations for the within-session repeatability measurement.

Magnetization prepared by ASL was imaged with a single-shot fast spin echo (SSFSE) acquisition. A 90° excitation pulse was followed by a pulse train of 130° flip angle pulses. The first two pulses, used to stabilize the echo train (29), were of flip angle 155° and 130°.

The 128×128 image matrix was acquired with $^{9}/_{16}$ partial-Fourier acquisition in the phase-encoded direction. A linear, near-center-outward phase ordering was used. A 40-cm field of view was covered with 10-mm slice thickness. TR/TE were 6000/50 ms, and the receiver bandwidth was ±19.23 kHz, with an echo spacing of 5.9 ms and total read-out time of 422 ms.

Total renal flow was measured in both renal arteries separately using an angiography sequence (30–32) to obtain an independent measurement of perfusion to the kidney. A spoiled gradient echo phase contrast sequence, with a flip angle of 20°, was used to acquire oblique-sagittal 2D images, of 7-mm thickness, 16-cm field of view and image matrix of 256 × 192, zero-padded to 256 × 256, centered on and perpendicular to the renal artery. The TR and TE were in the ranges 13–14 ms and 5–6 ms depending on pulse rate. Flow in all directions was encoded using a velocity encoding coefficient of v_{enc} = 100 cm/s. Peripheral cardiac gating was used to sort 20 measurements throughout the cardiac cycle. Imaging of all phases was performed within a single breath-hold of approximately 26 seconds.

Arterial Spin Labeling—Arterial spin labeling was performed using a pulsed-continuous labeling method (pCASL) (28,33), which permits continuous labeling (2,34) to be implemented using the body coil with the standard pulsed RF amplifiers for excitation instead of a separate transmit coil or amplifier. A train of short, closely spaced, radiofrequency pulses are played in the presence of a switching slice select gradient, which defines a labeling plane. A residual imbalance in the switching gradient imparts phase increments to spins within the vicinity of the labeling plane. For spins moving perpendicularly through the labeling plane, these phase increments evolve temporally between successive radiofrequency pulses, emulating a flow-driven adiabatic inversion of inflowing blood. Hann-shaped pulses of 0.5-ms duration, 3.56-kHz bandwidth, and maximum magnitude 0.07 G were played 1.166-ms apart in the presence of a gradient g_{max} = 0.7 G/cm. For pCASL labeling, the average radiofrequency over the pulse repetition period was $B_{1,av}$ = 0.015 G, and the average gradient over the same period was g_{av} = 0.1 G/cm. These parameters define a labeling plane of approximately 1.2-cm thickness and ensure adiabatic inversion for spins with a velocity perpendicular to the labeling plane of ≤ 200 cm/s. Previous simulations (28) have shown efficiency for pCASL inversion ≥ 0.8 for laminar flow with maximum speeds between 5 and 100 cm/s, and with similar pCASL gradient and RF parameters; the lower limit is mediated by T2-relaxation. The labeling plane was oriented axially at a distance of 8 cm from the center of the image field of view, approximately perpendicular to the aorta, and at the level of the diaphragm. Thus, spins in

NIH-PA Author Manuscript

NIH-PA Author Manuscript

NIH-PA Author Manuscript

blood were labeled in the descending aorta where blood flow is approximately plug-like with maximum velocities on the order of 100 cm/s (35–37).

Balancing the switching slice-select gradient and alternating the phase of the radiofrequency by π every successive pulse removes the phase increments accrued between pulses for moving spins resulting in a control condition for the ASL experiment. Magnetization transfer effects of the off-resonant radiofrequency applied at the imaging location are identical for both label and control conditions except very close to the labeling plane. Residual subtraction errors at the labeling plane permitted visualization of the labeling plane on the ASL difference images.

Spin labeling was applied for 1.5 s followed by a post-labeling delay (34) of 1.5 s before image acquisition. Label and control images were performed alternately during the multiple image acquisition to minimize subtraction errors.

Background Suppression—Background suppression (18–20) was achieved with a series of additional inversion and saturation pulses (Figure 1). Background signal was suppressed in an imaging region oriented axially, centered on the center of the coronally-orientated imaging slice, extending proximally to the labeling plane and an equal distance distally. The entirety of both kidneys was within the suppressed region. Suppression of signal was achieved by first selectively saturating the imaging region. The saturation pulses eliminate recovering magnetization from the previous repetition as well as begin the background suppression series of pulses. Four quadratic phase saturation pulses (38) were played 4.14 seconds prior to imaging (pulses were 10-ms duration, 12.5-kHz bandwidth and played 17 ms apart). Crusher-gradient pulses of incrementally increasing magnitude between the radiofrequency pulses were used to prevent refocusing of transverse magnetization. A selective “C-shape” FOCI inversion pulse (39), with duration 15.36 ms and bandwidth 1.08 kHz ($\beta = 509\ s^{-1}$ and $\mu = 6.2$) was then played immediately prior to labeling (3 seconds before imaging), inverting the imaging region. After 1.5 s of labeling, a series of non-selective adiabatic Hyperbolic-Secant inversion pulses (40) of 10-ms duration and 1.4-kHz bandwidth ($\beta = 970\ s^{-1}$ and $\mu = 4.5$) were applied. Two background suppression schemes were explored: i) heavy and ii) moderate. Heavy suppression was achieved with four non-selective inversion pulses applied at timings prior to image acquisition: 1491, 671, 239 and 48 ms; moderate suppression employed two inversion pulses at 1168 and 188 ms prior to imaging. Pulse timings were chosen to minimize the signal from a range of T1s between 250 and 4200 ms (41) using proprietary minimization routines available in the IDL Development Environment (ITT Visual Information Solutions, Boulder, CO) in a similar manner to that described elsewhere (19). Inclusion of inversion pulses leaves unaffected the difference between the magnetization of the label and control conditions (18). However, any inefficiency in the inversion pulses will diminish the difference between label and control conditions in the ASL experiment (22). Background suppression was quantified retrospectively by comparing the average signal intensity in a region of interest in the liver from images acquired with heavy and moderate background suppression to those with no background suppression pulses; estimates of signal suppression were averaged across the four subjects from images acquired in session 1 with timed breathing. Background signal was suppressed to 1.4 ± 0.1% and 11.0 ± 0.4%, for heavy and moderate schemes, respectively.

Without superior saturation, unsuppressed signal flowing into the slab after labeling produces a bright vascular signal that can contribute to subtraction errors. Inflowing arterial blood approaching from the superior side after the labeling period was suppressed by application of quadratic phase saturation pulses played during the interval between labeling and imaging, also followed by crusher-gradient pulses. For heavy background suppression,

NIH-PA Author Manuscript

NIH-PA Author Manuscript

NIH-PA Author Manuscript

three saturation pulses were played 1028, 383 and 62 ms before imaging; for moderate suppression, two saturation pulses at 1441 and 415 ms were played. The timing of the pulses was chosen such that the saturations, combined with subsequent inversions, would assure nullification of signals with the approximate T1 of blood at the imaging time. The saturation pulses were slab selective, 10-cm thick, in the axial orientation with distal edges coinciding with the labeling plane.

Reference Image Acquisition—Quantification of perfusion requires measurement of the fully relaxed magnetization signal, M_0, and the tissue T1. To enable quantification, perfusion acquisitions were begun with the acquisition of three reference images. These images used identical SSFSE acquisition but employed different magnetization preparation than the ASL. For each reference image, saturation was applied 4110 ms prior to image acquisition. The first image was acquired without any additional pulses. The second and third images were acquired with inversion pulses played after saturation, either 1560 or 180 ms before image acquisition. Inversion times were chosen to ensure longitudinal magnetization from all tissues was either positive or negative at excitation leading to smoothly varying phase in the image for partial Fourier reconstruction. Saturation consisted of two non-selective 10-ms duration, 12.5-kHz bandwidth quadratic phase saturation pulses, played 40-ms apart with gradient crushing of any transverse magnetization after each pulse. The inversion pulses were non-selective 15.36-ms duration, 1.08-kHz bandwidth adiabatic “C-shaped” FOCI pulses (39). These pulses are identical to saturation and inversion pulses used in the background suppression of the ASL preparation, except for the absence of gradients to impart spatial selectivity.

Respiratory Timing—Three breathing strategies were assessed that required different levels of cooperation from the subject. 1) *Multiple breath hold*. In this scheme, several breath-held acquisitions were required to obtain sufficient images for signal averaging. Each breath-held acquisition encompassed 3 or 4 image acquisitions lasting 18 or 24 seconds, respectively. Between breath-holds, approximately 2 minutes was allowed for the subject to recover normal breathing and prepare for the next acquisition. For each acquisition, the subject held their breath at end-expiration to improve reproducibility of the anatomic position of the kidneys during different acquisitions (42). 2) *Timed breathing*. This strategy requires cooperation from the subject to follow a simple, steady breathing pattern but does not require high respiratory capacity. The repetition time between image acquisitions was 6 seconds, which is consistent with a comfortable respiration rate. Subjects were asked to synchronize their breathing to the repetition time of the scanner by following the sounds produced by the switching gradients. The subject was asked to refrain from breathing at end expiration by the time of the successive image acquisition and to begin the next breath after completion of the data acquisition (the buzzing noise). The different noises of the image acquisition and ASL labeling were distinctive and assisted in following the desired pattern. Oftentimes it was observed from monitoring the trace from the respiratory bellows that expiration occurred during labeling. This gentle motion should not disturb the orientation of the aorta with respect to the axial labeling plane or the flow of blood along it, and therefore, this motion should have minimal effect on the flow-driven adiabatic inversion labeling process. 3) *Free breathing*. This strategy allowed the subject to breathe freely during acquisition of ASL images. For strategies 2 and 3, the subjects were asked to hold their breath for the acquisition of the reference images and then begin to breathe, either synchronized, or freely.

IMAGE ANALYSIS

Image Reconstruction—SSFSE data were saved as raw signal intensities to avoid the magnitude operation performed by the product reconstruction. Off-line reconstruction was

NIH-PA Author Manuscript

NIH-PA Author Manuscript

NIH-PA Author Manuscript

performed with custom programs in the IDL programming language (ITT Visual Information Solutions, Boulder, CO). *k*-Space was apodized with a circular Fermi filter with a sharp transition at 90% of the radius in *k*-space. A complex phase correction was applied to the image before half-Fourier reconstruction in *k*-space (43). Low spatial frequency phase variation across the image was estimated from the central portion of *k*-space (⅛ of the 128 phase encoded lines), apodized with a Hann function. ASL label-control pairs were subtracted and averaged in complex *k*-space prior to image reconstruction. Images from each element of the receiver array were combined using estimated coil sensitivities to prevent signal bias of the low signal-to-noise ratio perfusion signal. Coil sensitivities were estimated from the low resolution image from the central portion of *k*-space in each coil, corrected for low spatial frequency phase variation, and normalized with the root-sum-of-squares combination of low resolution images to remove the underlying spin density (44). Finally, images were interpolated to an image matrix of 256×256 by zero-padding in *k*-space.

Perfusion Quantification—The standard model for continuous labeling was adopted (2,34,45) for quantification of perfusion (Eq. [1]) where $\Delta M(t)$ is the difference in longitudinal magnetization between label and control images, t is the time of imaging after commencement of labeling, M_0 is the fully relaxed magnetization, λ is the blood-tissue partition coefficient, f is the flow (or perfusion), T_1' is the apparent time constant for relaxation of magnetization in the tissue (Eq. [2]), T_1 is the T1 of tissue, α is the inversion efficiency of the labeling pulses, Δt is the arrival time of labeled blood from the labeling plane to the tissue, $T_{1,\mathrm{blood}}$ is the T1 of arterial blood, and τ is the labeling time.

$$\Delta M(t)=2\frac{M_0}{\lambda}f\,T_1'\alpha\times\exp(-\Delta t/T_{1,\mathrm{blood}})\cdot\exp(-(t-\tau-\Delta t)/T_1')\times(1-\exp(-\tau/T_1')) \quad [1]$$

$$\frac{1}{T_1'}=\frac{1}{T_1}+\frac{f}{\lambda} \quad [2]$$

In our study, the labeling time τ was 1.5 s. The arrival time Δt was assumed to be 750 ms (11) for blood to travel 80 mm in the aorta (the approximate distance from the labeling plane to the level of the renal arteries) before branching into the renal arteries and arriving at the renal tissue. A post-labeling delay of 1.5 s was used so that the measurement time (t = 3 s) occurs after the arrival of all labeled blood. The perfusion signal is thus not strongly affected by small changes in the arrival time Δt. For T_1 = 1 s and $T_{1,\mathrm{blood}}$ = 1.3 s, the fractional change in the perfusion signal is given by: $\partial\Delta M/\Delta M \approx \partial\Delta t\times 0.2\mathrm{sec}^{-1}$, which for $\partial\Delta t \approx 50$ ms, is approximately 1%. A typical value of 0.9 was assumed for the blood-tissue water partition coefficient, λ, as previously measured in the brain (46), and which has also previously been assumed for abdominal tissues, including the renal cortex (47) and skeletal muscle (48). A value of 1.3 s was used for the T1 of blood (34,49). For an anticipated maximum flow $f \approx 500$ mL / 100 g · min, and λ = 0.9, the ratio $f/\lambda \approx 0.1\ \mathrm{s}^{-1}$, which is sufficiently smaller than $1/T_1 \approx 1\ \mathrm{s}^{-1}$ to assume that $T_1' \approx T_1$. The efficiency of the pulsed-continuous labeling was estimated at approximately 0.8 based on previous simulations (28). The efficiency of the labeling is reduced further by the inefficiency of the background suppression inversion pulses experienced by the labeled spins. Previous work (22) has shown that a series of four (or two) adiabatic inversion pulses used for background suppression, similar to those used here, have an estimated efficiency, in vivo, of 0.75 (or 0.87). Thus, the combined inversion efficiency, α, for the pulsed-continuous labeling with

NIH-PA Author Manuscript

NIH-PA Author Manuscript

NIH-PA Author Manuscript

heavy four-pulse background suppression for our experiment was estimated to be 0.6, for moderate 2-pulse suppression, it was 0.69, and for no background suppression, it was 0.8.

Proton density and tissue T1 values used in the quantification were measured from the reference images acquired concurrently with the perfusion measurement. A saturation recovery and two inversion recovery images were acquired at the start of the perfusion imaging sequence without labeling or background suppression pulses; saturation and inversion pulses were applied at times t_{sat} and TI before imaging, respectively. T1 was calculated by fitting the pixel values from the two inversion recovery images, each normalized by the pixel value of the saturation recovery image, to the signal equation

$$\frac{M_{inv}(TI)}{M_{sat}} = \frac{1+\exp(-t_{sat}/T_1) - 2\exp(-TI/T_1)}{1-\exp(-t_{sat}/T_1)}. \quad [3]$$

The use of the reference image, M_{sat}, to estimate the fully relaxed blood magnetization in the quantification also corrects signal intensity variations due to the sensitivity of the coil elements in the receiver array and additional T2 contrast arising from the SSFSE acquisition.

To avoid creating quantitative perfusion images visually dominated by noise outside perfused tissues, masking of regions with low T1 or proton density signal intensity was performed. The uniform noise throughout the perfusion difference image is scaled by the proton density and measured tissue-T1 values upon quantification of perfusion. Outside the kidney, where signal is low in muscle and T1 is short in fat, noise in the calculated perfusion is greater than within the kidney. To prevent the appearance of this noise from dominating the appearance of the actual noise of quantified perfusion values within the kidney, T1 values lower than 700 ms outside the kidney (which is assumed to be lower than T1 for cortex and medulla within the kidney) were set to this threshold for quantification. Additionally, a mask of the body was applied throughout quantification to remove background air.

All image reconstruction, perfusion quantification and processing was carried out off-line using in-house programs written in the IDL Development Environment (ITT Visual Information Solutions, Boulder, CO).

Total Renal Flow – MRA—Total renal flow was measured (30–32) to identify gross difference in the renal flow between test and retest for each subject and therefore to correct for such a bias in the test-retest calculation. ROIs were manually drawn around the lumen of the renal artery on the calculated velocity image for every cardiac phase point. Instantaneous volume flow rate at each point in the cardiac cycle was the summation of pixel velocities within the ROI, multiplied by the pixel area (3.9×10^{-3} cm^2). Total renal flow was calculated by averaging volume flow rate over the 20 phases of the cardiac cycle. The change in measured total renal flow between test and retest was plotted against the change in measured perfusion and the correlation coefficient found to determine whether correction for physiological differences in renal flow between test and retest would be beneficial. In addition, the correlation between measured total renal flow and perfusion was calculated.

Absolute values of total renal blood flow were compared to values expected from the literature. In addition, total renal flow was estimated from the measured average perfusion to the kidney. Quantitative perfusion values were averaged across the whole slice for both kidneys in all four subjects in session 1 of Study 1 (for the measurements made with timed breathing and heavy background suppression; (Ai) above). In addition, the average number of pixels in the ROIs covering both kidneys was found, and, with the pixel size (0.0244 cm^2)

NIH-PA Author Manuscript

NIH-PA Author Manuscript

NIH-PA Author Manuscript

and slice thickness (1 cm), the average volume of renal tissue (for both kidneys) was estimated in which perfusion was measured. Multiplying these values together gave an estimate of the total flow to this slice of the kidney in units of L/min that could be compared to the total renal flow to the whole kidney as measured by phase-contrast MRA.

Background Suppression and Breathing Strategies (STUDY 1)—The improvement in image quality after applying breathing strategies and background suppression was assessed by measuring two quantities: i) the test-retest repeatability, COV_F, of the total perfusion, and ii) the standard deviation of perfusion values within ROIs encompassing either cortical or medullary tissues. This standard deviation includes all sources of noise, including artifactual motion related noise, and, therefore, changes in the latter were indicated by changes in the ROI-standard deviation. COV_F was calculated from the "whole-slice" average flow in both cortex and medulla, F_{WS}. F_{WS} was measured from pixel values within manually drawn ROIs around the borders of the whole kidney on the quantitative perfusion image. F_{WS} was treated as a normally distributed quantity with a mean that varies between subjects but whose variance, σ^2_F, is the same for all subjects. Measurements at test and retest were considered to be independent measurements of the same distribution. The difference between F_{WS} at test and retest, δF_{WS}, was found for each kidney in all subjects (8 kidneys in total). The variance of flow measurements, $\sigma^2_F = \mathrm{var}(F_{WS})$ was then estimated from the variance of differences δF_{WS}, averaging over subjects, according to $\mathrm{var}(\delta F_{WS}) = 2\times\mathrm{var}(F_{WS})$. Finally, the test-retest repeatability, COV_F, was the standard deviation of the measured perfusion, F_{WS}, expressed as a percentage of the average of F_{WS} over all kidneys, $COV_F = (\sigma_F/\mathrm{mean}(F_{WS}))\times 100\%$. COV_F was calculated for each combination of breathing strategy and background suppression. An *F*-test for significant differences in the variances of the perfusion measurements was performed between all pairs of combined strategies, based on $\mathrm{var}(\delta F_{WS})$ (50).

Segmentation of renal cortex and medulla was performed to facilitate the quantitative assessment of image artifacts by measuring the standard deviation in the distribution of flow values about the mean within an ROI encompassing the same tissue. Within the ROI of the whole kidney used above, cortex was segmented from medulla according to the measured T1 of tissue. T1 values less than 1150 ms were assigned to be cortex and above were deemed to be medulla. The threshold value (1150 ms) was chosen in accordance with literature values (51), and was adjusted to result in approximately 50/50 division between cortex and medulla according to a reasonable proportion of the tissue types in normal kidneys (52). Significant differences in these ROI-standard deviation values between strategies were sought. Welch's *t*-test was used to compare between strategies because each strategy may have measurements of perfusion with distributions of unequal variance. The statistic *t* and the significance *p*-value for a two-tailed test were calculated from the mean values and standard deviations of the quantity *ROI-standard deviation*, averaging over both kidneys of all subjects from both sessions (16 measurements in total) for measurement strategy "A" and "B". Comparisons were made pair-wise between strategies for cortical and medullary tissues separately (50). To estimate the Gaussian, thermal noise contribution to SNR we defined an ROI outside of the object, away from any gross motion related artifacts. The standard deviation of the signal within the ROI on the perfusion difference images was calculated. These images were complex coil-combined to reduce bias error (53). Still, the standard deviation cannot be easily related to the noise in the kidney perfusion signal because of differences in the coil sensitivities and their combinations at the two different locations. Instead, this regional standard deviation serves as a relative estimate of thermal noise in the images for comparison between different acquisition strategies. We compared the relative SNR per square root of acquisition time, rSNRrt, calculated for the average perfusion difference signal in the renal cortex, between the acquisition strategies. The

NIH-PA Author Manuscript

NIH-PA Author Manuscript

NIH-PA Author Manuscript

statistic *t* and the significance *p*-value were found for a two-tailed test between strategies, averaging over rSNRrt measurements in both kidneys of all subjects in one of the sessions.

In addition to quantitative assessment described above, subjective image quality was assessed separately by two radiologists (I.P. and N.M.R.) blinded to acquisition strategy. Perfusion difference images were assessed for i) the severity of artifacts and their propensity to obscure high/low perfusion features in the kidney; ii) the overall image quality, including the appearance of SNR and image blurring as well as the appearance of artifacts. Rating for question i) was on the following scale: 1) extremely poor, artifacts obscure most parts of the kidney; 2) poor, artifacts obscure parts of the kidney; 3) good, minor troubling artifacts; 4) very good, the kidney is well observed. For question ii), rating was: 1) extremely poor, would not be confident to identify regions of abnormal flow; 2) poor, expect to be able to identify major features of abnormal flow; 3) good, would be confident to identify major regions of abnormal flow but not confident to identify subtle features; 4) very good, confident to identify all features of abnormal flow. For each combined strategy, the average score over all subjects was found. Using a Mann-Whitney U-test, significant tendencies for one strategy to score higher than another were sought. Each strategy was compared pair-wise to every other. In addition, the correlation of scoring between the two radiologists was tested with a Spearman rank correlation coefficient (50).

Retrospective Respiratory Sorting (STUDY 2)—Image data from this second part of the study was examined as for the first. The ("in-session") test-retest value, COV_F, for the whole-slice average flow, F_{WS}, was calculated for the timed breathing scans (measurements (G) described above) and for the free breathing data (measurements (F)) processed with each of the retrospective sorting strategies. Then, pair-wise for all data sets, an *F*-test was used to assess significant differences in measurement variance. Significant differences were sought between the ROI-standard deviations of perfusion values for all pairs of strategies, to indicate changes in the artifactual motion related noise, which contributes to the ROI-SD. Regions of cortex and medulla were treated separately, segmented according to measured T1 of tissue. Estimating the contribution of thermal noise, measurements of the relative SNR, rSNRrt, were also made, calculated on the perfusion difference images, and compared between sorting strategies.

Perfusion difference images, with and without retrospective sorting, were also assessed separately by the two radiologists (I.P. and N.M.R.) who were asked to choose the image that showed: i) better sharpness, and ii) better SNR. The readers were blinded to which images were sorted and which were not. Eight pairs of images from the test and retest of the four subjects were assessed. In each pair, the order of showing the sorted and unsorted images was randomized. The perfusion images calculated by averaging those images acquired closest to end-expiration were used.

Results

STUDY 1: Background Suppression and Breathing Strategies

High quality ASL images were obtained in all subjects for some of the combinations of background suppression and breathing strategy but not others. Quantitative assessment of these strategies revealed test-retest repeatability, COV_F, between sessions a week apart was typically 10–20%, for all strategies (Table 1). The lowest values for the test-retest repeatability, COV_F were 7% and 8% for heavy background suppression combined with breath-holding, and the in-session comparison of the timed breathing strategy with heavy background suppression. The *F*-tests showed significant differences in the variance of these measurement strategies. The strategy with heavy background suppression and breath-holds was significantly better than any other strategy at the 5% level, or better. The in-session

NIH-PA Author Manuscript

NIH-PA Author Manuscript

NIH-PA Author Manuscript

measurement was significantly better (10% level, or better) compared to most other strategies, except the breath-holding strategies with background suppression. Other significant results found were at the 5–10% level, but were not consistently significant across all comparisons. No other significant differences were found indicating that variability between sessions, such as repositioning the slice or physiological changes, dominates variability due to the imaging strategy in most cases.

Comparing ROI standard deviation between combined strategies, images without any background suppression (acquired only with timed breathing) were significantly poorer ($p < 0.05$) when compared to all other combinations of background suppression and breathing strategy (Table 2), indicating an elevated level of artifactual motion related noise. Comparisons between all other pairs of combined strategies involving one common breathing or background suppression scheme revealed no significant differences (Table 2). Measurements of the relative SNR, rSNRrt, revealed no significant differences between strategies. A typical value of the relative SNR for the renal cortex in the perfusion difference images, averaged over 16 label-control pairs, was 15 (i.e. rSNRrt $\times \sqrt{32} \approx 15$). Without background suppression pulses, where the signal is expected to be slightly greater (inefficiency of inversion pulses), the lack of change in rSNRrt is assumed to be due to a corresponding increase in artifactual motion related noise, concomitant to the absence of background suppression.

Average reader scores of image quality, shown in Figure 2, indicate a clear preference for background suppression, and a slight preference for timed breathing, from both radiologists for reducing the appearance of artifacts and improving the overall image quality. Mann-Whitney U-tests between strategies (two-sided at the 5% level) showed some differences between the radiologists; significant differences were found between different pairs of strategies. Significant differences were found by both radiologists and for both questions in favor of background suppression when comparing the strategy with no background suppression and timed breathing to i) heavy and ii) moderate background suppression, both with timed breathing. For all other comparisons involving the strategy without background suppression, a significant difference in favor of using background suppression was found by one or other of the radiologists. No other trends in the remaining significant results were discernible. The correlations between the radiologists' scores were significant, with a two-sided p-value < 0.05 (Spearman rank correlation) for both questions pertaining to: i) artifact and ii) overall quality. Although some differences in scoring were evident, no images were scored highly by one reader and lowly by the other.

A typical, high quality perfusion difference image and a quantitative perfusion map are shown in Figure 3 acquired with heavy background suppression and multiple breath-holds. The images show excellent distinction between areas of high and low perfusion, which correspond to cortex and medulla, respectively. Typical images acquired with timed and free breathing strategies with heavy background suppression (all images are from subject 1) are also shown in Figure 3, showing the benefit of using a breathing strategy to mitigate image-blurring by large-scale motion during imaging due to respiration. It can be noted that the quantitative image acquired with the timed breathing strategy shows a hyper-intense edge artifact due to misalignment of the perfusion difference image and the reference images used in quantification. Figure 4 shows perfusion difference images for each of the combinations of breathing strategy and background suppression acquired; all images were acquired in subject 2. Figure 4 also shows two additional images acquired in this one volunteer without any background suppression inversion pulses and with the breath-hold, and free breathing schemes indicating the severe artifacts that are greatly reduced by using background suppression pulses.

NIH-PA Author Manuscript

NIH-PA Author Manuscript

NIH-PA Author Manuscript

Quantitative flow values found from Study 1 were (range; mean ± SD): *Whole Kidney* (231–601; 332 ± 140) mL / 100 g · min; *Cortex* (287–706; 410 ± 150) mL / 100 g · min; *Medulla* (165–346; 223 ± 76) mL / 100 g · min. These values are in agreement with other recent studies of perfusion in the kidneys employing ASL (11,12,15).

The efficiency of inversion pulses used for background suppression is known to be imperfect (22). This has the effect of reducing the perfusion signal (difference between labeled and unlabeled magnetization) available for imaging and consequently reducing the perfusion difference signal and perfusion map SNR. Reduction depends on the number of inversion pulses experienced by labeled spins. In the raw perfusion difference images acquired with the timed breathing strategy, the average signal within the ROI of the whole kidney was measured and averaged over left and right kidneys of all subjects. For heavy and moderate background suppression with four and two pulses, respectively, the signal was reduced by 23% and 16% with respect to the signal without background suppression.

TOTAL RENAL FLOW

Phase contrast measurements of the total renal flow in each kidney showed good correlation with average perfusion measured by ASL. The slope and intercept of a scatter plot (Figure 5a) between perfusion flow and phase-contrast measurements for both kidneys in four subjects for both test and retest were 29 ± 10 (mL/100g.min)/(mL/s) and 28 ± 111 (mL/100g.min)/(mL/s). The correlation coefficient R was equal to 0.61, which was significant at the 5% level. There was no significant correlation ($R = 0.1$) in the differences of measurements at test and retest between measured perfusion and total renal flow (Figure 5b). Therefore, phase-contrast measurements were not used to apply a correction for gross changes in total renal flow between test and retest.

A quantitative measurement of the agreement between perfusion and MRA measurements of total renal flow was made and compared to literature values for renal blood flow. Average total renal blood flow to both kidneys measured by phase contrast MRI was 1.3 L/min, which is consistent with total renal flow comprising approximately 25% of cardiac output, itself, approximately 5–6 L/min (52), and is also consistent with previous MR measurements (31). Average perfusion to the kidney was also found to be consistent with expected total renal blood flow. The average perfusion to a pixel was estimated to be 332 mL / 100 g · min, and the average volume of renal tissue (in both kidneys) in which perfusion was measured was estimated to be 95 mL. This gives an estimate of the total flow into the slice, measured by perfusion, to be 0.32 L/min. The ratio 0.32/1.3 is a reasonable figure for the fraction of the volume of the kidneys measured by perfusion.

STUDY 2: Retrospective Respiratory Sorting

The within-session test-retest values, COV_F, for each of the retrospective sorting schemes employed were distributed in the range 1.7% to 6.8% (Table 3) around the value obtained from the timed breathing of 6.6% (standard deviation of the whole-slice perfusion value, expressed as a percentage of the whole-slice average flow.) The lowest value of COV_F (1.7%) was found for the sorting strategy taking image-averages closest to end expiration. The F-tests revealed a significantly lower measurement variance (at the 1% and 5% levels, respectively) for the images that included sorting based on selecting the image-averages closest to end-expiration, or closest together in bellows position, compared to all other strategies (except at the 10% level when compared to each other). No significant differences in the ROI-standard deviation of perfusion values were found between the timed breathing strategy and any scheme of retrospective sorting of free-breathing data (Table 4). Significant differences were not found between any pair of retrospective sorting schemes.

NIH-PA Author Manuscript

NIH-PA Author Manuscript

NIH-PA Author Manuscript

Measurements of the relative SNR, rSNRrt, also showed no significant differences between any two strategies.

Images reconstructed with one portion of the free breathing data replaced with data acquired when the subject was asked to take deep breaths during imaging showed the extent to which final perfusion images may be corrupted by occasional erratic breathing during a free-breathing experiment. Implementing the retrospective sorting scheme that accepts reference images and ASL images with bellows positions closest to end-expiration (the best test-retest repeatability, COV_F) demonstrates an appreciable improvement in image quality. Boundaries between regions of high and low perfusion, corresponding to cortical and medullary tissue, are much sharper after retrospective image sorting, as shown in Figure 6. Image assessment by the radiologists of these images before and after sorting confirmed this finding. Both readers found 100% of the images with sorting were preferable for image sharpness. For SNR, one radiologist preferred 100% of the images without any sorting, while the other found 88% of the images without sorting preferable and 12% (one image) with sorting preferable.

Discussion

Findings from quantitative measures of the images and from assessments by the radiologists are generally in agreement. There is a clear preference for background suppression, with little significant discrimination between other combinations of background suppression and breathing strategies. We surmise that the quantitative measurements of the mean and standard deviation of flow values within ROIs are unsuitable for detecting artifactual corruption of the image. Edge artifacts from misaligned label-control pairs or repetitions, or image ripples and other corruptions from *k*-space errors arising from unsuppressed physiologic noise tend to average toward the true value that would be obtained by that strategy if it were suffering no respiratory motion artifacts. The importance of background suppression is made apparent, qualitatively, by the low measurement variance and high reader-rating found for images acquired during free breathing when background suppression was used.

Physiologic variation of renal flow may have contributed to the test-retest variability of the results. The timing and content of recent meals, especially protein content (54), can have a substantial effect on renal blood flow. No control for eating prior to imaging was used for this initial study. Variability in measured total flow may also have arisen from placement of the imaging slice through the kidneys leading to variable volumes of perfused parenchyma being included. Additionally, variability in measured total flow between test and retest may have been introduced through variable inversion efficiency as a function of changing blood flow speed or pulsatility in the aorta, or from off-resonance effects from residual field inhomogeneity differing due to patient positioning and/or shimming. Such sources of variability may have overshadowed variability due to the background suppression and breathing strategy acquisition schemes.

In our experience, when a subject follows a multiple breath-hold, or timed breathing scheme well, as monitored by the respiratory bellows position, the resulting images are most often of superior quality. However, no statistical preference for breathing strategies was found. Each breathing strategy has advantages and disadvantages, which may have compensated for one another under statistical analysis. Observation of breathing in our subjects indicates that multiple breath-hold acquisitions most often result in a consistent end-expiration position, which is favorable for restricting respiratory motion between repetitions. However, the breath-hold procedure requires additional time between acquisitions resulting in fewer averages being acquired in the same time compared to the timed and free breathing

NIH-PA Author Manuscript

NIH-PA Author Manuscript

NIH-PA Author Manuscript

strategies, even accounting for image rejection. In addition, breath-holding may be impossible with some patients. The timed breathing strategy, when followed effectively, produces images of comparable quality to breath-held acquisition with additional benefit of a higher signal-to-noise ratio per imaging time. However, even with cooperative volunteers we found that the breathing scheme was not maintained well throughout all scans. When asked to breathe freely, subjects most often fall into a gentle shallow breathing pattern resulting in only small displacements between repeated acquisitions. In comparison, when conscious of following a breathing pattern (timed breathing) subjects are prone to taking sharper deep breaths. For a patient population where breath-held acquisition is not likely and timed breathing is unlikely to be followed well, our experience from clinical populations (not reported here) has indicated a suitable compromise: repeated, shallow, 6-s breath-holds for reference scans at the beginning of the scan followed by shallow free breathing. This is most likely to produce robust calculation of the T1 and M_0 maps required for perfusion quantification and produce minimal disruption to the ASL difference image. Any periods of erratic breathing that induce large abdominal displacements are effectively dealt with using retrospective respiratory sorting. However, it is also useful to include additional reference image acquisitions during the remainder of the scan.

Retrospective sorting of image acquisitions based on respiratory position enables images without gross motion related artifact to be obtained with free breathing at the expense of lower signal-to-noise ratio resulting from image rejection. Typically, accepting half of the acquired images is offset by the possibility of acquiring data twice as long. The ease of preparation for imaging without breath-holding or timing breathing enables more time to be spent acquiring data. The acceptance criterion may be adjusted to trade off loss in signal-to-noise ratio for reduced image degradation due to motion. It is useful to reconstruct images both with sorting and using all available image acquisitions for comparison. Our initial study of retrospective sorting has used the respiratory bellows position to indicate the position of the kidneys. However, other techniques, including navigators, may prove more accurately correlated indicators of position (55). More sophisticated motion-monitoring schemes may also prove useful. For example, each raw label and control image, or additional structural images, could be used in registration algorithms, although issues of image SNR, and acquisition time become important, as well as the possibility of non-rigid body motions.

Perfusion difference images were most often of high quality. The additional image-processing required to compute quantitative perfusion maps occasionally degraded image quality due to miss-registration between the perfusion difference image and the reference images used to calculate tissue-T1 and estimate relaxed blood magnetization in the quantification.

Whilst this study was carried out at 1.5 T, renal perfusion measurements at 3 T, where perfusion studies benefit from intrinsically higher SNR and longer T1 values, will also benefit from the respiratory motion artifact-reduction strategies described here. Background suppression pulse timings can be easily recalculated for different T1-relaxation rates, and their power deposition, despite being adiabatic in nature, is not a great concern over the course of the labeling and imaging cycle. pCASL labeling itself may be more problematic in the abdomen at increased field strength, where B1-inhomogeneity may cause inefficiencies in the labeling. Main-field inhomogeneity may also pose similar problems; however, studies in the brain have proven successful (28).

Our focus in this study was more on reducing subtraction error due to motion of the background than on eliminating motion related degradation of the perfusion signal. In the absence of background subtraction error, the averaging of multiple images at slightly different positions is likely to cause blurring of the perfusion signal. If multi-shot imaging

NIH-PA Author Manuscript

NIH-PA Author Manuscript

NIH-PA Author Manuscript

sequences are used, as might be desirable for 3-D imaging, then motion could also cause more complex artifacts linked to the phase acquisition order.

The successful application of abdominal ASL has merit in providing an alternative to gadolinium based contrast media for characterizing masses (56–58), assessing organ perfusion (59,60), and assessing tumor response to certain therapies, particularly those that are anti-angiogenic (61,62). The techniques described herein, offer abdominal ASL studies of a quality to be considered reasonable for clinical use.

Conclusion

High quality quantitative renal perfusion imaging has been demonstrated using Arterial Spin Labeling. Average perfusion was measured to be 332, 410, and 223 mL / 100 g · min in the whole kidney, cortex, and medulla, respectively. Within-session repeatability was measured to be 8%, which was significantly lower than typical between-session repeatability, found to be in the range 10–20%. Image quality was most significantly improved by using background suppression schemes employing multiple inversion pulses. This was demonstrated with statistical significance both from measurement variance and assessment by radiologists. Background suppression, without compensating exactly for motion, reduces subtraction artifacts in the background signal to a tolerable level, small compared to the perfusion signal, making the ASL measurement robust to both physiological motions and bulk motion due to respiration during free breathing acquisitions resulting in acceptable image quality. Image quality was observed to be improved by controlling respiratory motion with the timed breathing strategy when assessed qualitatively by radiologists, although a significant difference in the quantitative measurements of test-retest repeatability was not found. SNR efficiency may be optimized by employing a patterned, timed breathing approach. In a clinical setting, the ability to implement retrospective image sorting will improve the image quality of ASL in the abdomen acquired during free breathing. Significant reduction in measurement variance, compared to other sorting schemes or a timed breathing scheme, was found by accepting only images acquired closest to end-expiration. Using the position of the respiratory bellows has proven successful in this study.

Acknowledgments

This work was supported in part by the National Institutes of Health through National Cancer Institute grant CA121570.

References

1. Detre JA, Leigh JS, Williams DS, Koretsky AP. Perfusion imaging. Magn Reson Med. 1992; 23(1): 37–45. [PubMed: 1734182]
2. Williams DS, Detre JA, Leigh JS, Koretsky AP. Magnetic resonance imaging of perfusion using spin inversion of arterial water. Proc Natl Acad Sci U S A. 1992; 89(1):212–216. [PubMed: 1729691]
3. Kwong KK, Belliveau JW, Chesler DA, Goldberg IE, Weisskoff RM, Poncelet BP, Kennedy DN, Hoppel BE, Cohen MS, Turner R, et al. Dynamic magnetic resonance imaging of human brain activity during primary sensory stimulation. Proc Natl Acad Sci U S A. 1992; 89(12):5675–5679. [PubMed: 1608978]
4. Edelman RR, Siewert B, Adamis M, Gaa J, Laub G, Wielopolski P. Signal targeting with alternating radiofrequency (STAR) sequences: application to MR angiography. Magn Reson Med. 1994; 31(2): 233–238. [PubMed: 8133761]
5. Edelman RR, Siewert B, Darby DG, Thangaraj V, Nobre AC, Mesulam MM, Warach S. Qualitative mapping of cerebral blood flow and functional localization with echo-planar MR imaging and

NIH-PA Author Manuscript

NIH-PA Author Manuscript

NIH-PA Author Manuscript

signal targeting with alternating radio frequency. Radiology. 1994; 192(2):513–520. [PubMed: 8029425]

6. Kim SG. Quantification of relative cerebral blood flow change by flow-sensitive alternating inversion recovery (FAIR) technique: application to functional mapping. Magn Reson Med. 1995; 34(3):293–301. [PubMed: 7500865]
7. Wong EC, Buxton RB, Frank LR. Implementation of quantitative perfusion imaging techniques for functional brain mapping using pulsed arterial spin labeling. NMR Biomed. 1997; 10(4–5):237–249. [PubMed: 9430354]
8. Alsop DC, Detre JA. Multisection cerebral blood flow MR imaging with continuous arterial spin labeling. Radiology. 1998; 208(2):410–416. [PubMed: 9680569]
9. Alsop DC, Detre JA, Grossman M. Assessment of cerebral blood flow in Alzheimer's disease by spin-labeled magnetic resonance imaging. Ann Neurol. 2000; 47(1):93–100. [PubMed: 10632106]
10. Duyn JH, van Gelderen P, Talagala L, Koretsky A, de Zwart JA. Technological advances in MRI measurement of brain perfusion. J Magn Reson Imaging. 2005; 22(6):751–753. [PubMed: 16267852]
11. Roberts DA, Detre JA, Bolinger L, Insko EK, Lenkinski RE, Pentecost MJ, Leigh JS Jr. Renal perfusion in humans: MR imaging with spin tagging of arterial water. Radiology. 1995; 196(1): 281–286. [PubMed: 7784582]
12. Karger N, Biederer J, Lusse S, Grimm J, Steffens J, Heller M, Gluer C. Quantitation of renal perfusion using arterial spin labeling with FAIR-UFLARE. Magn Reson Imaging. 2000; 18(6): 641–647. [PubMed: 10930773]
13. Martirosian P, Klose U, Mader I, Schick F. FAIR true-FISP perfusion imaging of the kidneys. Magn Reson Med. 2004; 51(2):353–361. [PubMed: 14755661]
14. De Bazelaire C, Rofsky NM, Duhamel G, Michaelson MD, George D, Alsop DC. Arterial spin labeling blood flow magnetic resonance imaging for the characterization of metastatic renal cell carcinoma(1). Acad Radiol. 2005; 12(3):347–357. [PubMed: 15766695]
15. Fenchel M, Martirosian P, Langanke J, Giersch J, Miller S, Stauder NI, Kramer U, Claussen CD, Schick F. Perfusion MR imaging with FAIR true FISP spin labeling in patients with and without renal artery stenosis: initial experience. Radiology. 2006; 238(3):1013–1021. [PubMed: 16439565]
16. Gach H, Nguyen T, Wang Y. CASL Perfusion MRI of the Kidney using Real-time Tracking, Free Breathing Navigator. Proc ISMRM. 2006:2990.
17. Kuo PH, Kanal E, Abu-Alfa AK, Cowper SE. Gadolinium-based MR contrast agents and nephrogenic systemic fibrosis. Radiology. 2007; 242(3):647–649. [PubMed: 17213364]
18. Dixon WT, Sardashti M, Castillo M, Stomp GP. Multiple inversion recovery reduces static tissue signal in angiograms. Magn Reson Med. 1991; 18(2):257–268. [PubMed: 2046511]
19. Mani S, Pauly J, Conolly S, Meyer C, Nishimura D. Background suppression with multiple inversion recovery nulling: applications to projective angiography. Magn Reson Med. 1997; 37(6): 898–905. [PubMed: 9178242]
20. Ye FQ, Frank JA, Weinberger DR, McLaughlin AC. Noise reduction in 3D perfusion imaging by attenuating the static signal in arterial spin tagging (ASSIST). Magn Reson Med. 2000; 44(1):92–100. [PubMed: 10893526]
21. St Lawrence KS, Frank JA, Bandettini PA, Ye FQ. Noise reduction in multi-slice arterial spin tagging imaging. Magn Reson Med. 2005; 53(3):735–738. [PubMed: 15723412]
22. Garcia DM, Duhamel G, Alsop DC. Efficiency of inversion pulses for background suppressed arterial spin labeling. Magn Reson Med. 2005; 54(2):366–372. [PubMed: 16032674]
23. Runge VM, Clanton JA, Partain CL, James AE Jr. Respiratory gating in magnetic resonance imaging at 0.5 Tesla. Radiology. 1984; 151(2):521–523. [PubMed: 6709928]
24. Schultz CL, Alfidi RJ, Nelson AD, Kopiwoda SY, Clampitt ME. The effect of motion on two-dimensional Fourier transformation magnetic resonance images. Radiology. 1984; 152(1):117–121. [PubMed: 6729101]
25. Ehman RL, Felmlee JP. Adaptive technique for high-definition MR imaging of moving structures. Radiology. 1989; 173(1):255–263. [PubMed: 2781017]

NIH-PA Author Manuscript NIH-PA Author Manuscript NIH-PA Author Manuscript

26. Liu YL, Riederer SJ, Rossman PJ, Grimm RC, Debbins JP, Ehman RL. A monitoring, feedback, and triggering system for reproducible breath-hold MR imaging. Magn Reson Med. 1993; 30(4): 507–511. [PubMed: 8255201]
27. Martirosian P, Boss A, Fenchel M, Deimling M, Schafer J, Claussen CD, Schick F. Quantitative lung perfusion mapping at 0.2 T using FAIR True-FISP MRI. Magn Reson Med. 2006; 55(5): 1065–1074. [PubMed: 16602073]
28. Dai W, Garcia DM, De Bazelaire C, Alsop D. Continuous Flow Driven Inversion for Arterial Spin Labeling Using Pulsed Radiofrequency and Gradient Fields. Magn Reson Med. 2008 in press.
29. Alsop DC. The sensitivity of low flip angle RARE imaging. Magn Reson Med. 1997; 37(2):176–184. [PubMed: 9001140]
30. Pelc LR, Pelc NJ, Rayhill SC, Castro LJ, Glover GH, Herfkens RJ, Miller DC, Jeffrey RB. Arterial and venous blood flow: noninvasive quantitation with MR imaging. Radiology. 1992; 185(3):809–812. [PubMed: 1438767]
31. Debatin JF, Ting RH, Wegmuller H, Sommer FG, Fredrickson JO, Brosnan TJ, Bowman BS, Myers BD, Herfkens RJ, Pelc NJ. Renal artery blood flow: quantitation with phase-contrast MR imaging with and without breath holding. Radiology. 1994; 190(2):371–378. [PubMed: 8284383]
32. King BF, Torres VE, Brummer ME, Chapman AB, Bae KT, Glockner JF, Arya K, Felmlee JP, Grantham JJ, Guay-Woodford LM, Bennett WM, Klahr S, Hirschman GH, Kimmel PL, Thompson PA, Miller JP. Magnetic resonance measurements of renal blood flow as a marker of disease severity in autosomal-dominant polycystic kidney disease. Kidney Int. 2003; 64(6):2214–2221. [PubMed: 14633145]
33. Garcia DM, De Bazelaire C, Alsop D. Pseudo-Continuous Flow Driven Adiabatic Inversion for Arterial Spin Labeling. Proc ISMRM. 2005:37.
34. Alsop DC, Detre JA. Reduced transit-time sensitivity in noninvasive magnetic resonance imaging of human cerebral blood flow. J Cereb Blood Flow Metab. 1996; 16(6):1236–1249. [PubMed: 8898697]
35. Klipstein RH, Firmin DN, Underwood SR, Rees RS, Longmore DB. Blood flow patterns in the human aorta studied by magnetic resonance. Br Heart J. 1987; 58(4):316–323. [PubMed: 3676019]
36. Matsuda T, Shimizu K, Sakurai T, Fujita A, Ohara H, Okamura S, Hashimoto S, Tamaki S, Kawai C. Measurement of aortic blood flow with MR imaging: comparative study with Doppler US. Radiology. 1987; 162(3):857–861. [PubMed: 3544040]
37. Maier SE, Meier D, Boesiger P, Moser UT, Vieli A. Human abdominal aorta: comparative measurements of blood flow with MR imaging and multigated Doppler US. Radiology. 1989; 171(2):487–492. [PubMed: 2649924]
38. Kunz D. Frequency-modulated radiofrequency pulses in spin-echo and stimulated-echo experiments. Magn Reson Med. 1987; 4(2):129–136. [PubMed: 3561242]
39. Ordidge RJ, Wylezinska M, Hugg JW, Butterworth E, Franconi F. Frequency offset corrected inversion (FOCI) pulses for use in localized spectroscopy. Magn Reson Med. 1996; 36(4):562–566. [PubMed: 8892208]
40. Silver M, Joseph R, Hoult D. Highly Selective pi/2 and pi Pulse Generation. Journal of Magnetic Resonance. 1984; 59:347–351.
41. Maleki N, Dai W, Alsop D. A Systematic Approach to Optimizing Background Suppression for Arterial Spin Labeling Perfusion Imaging. Proc ISMRM. 2008:1929.
42. Zhang J, Pedrosa I, Rofsky NM. MR techniques for renal imaging. Radiol Clin North Am. 2003; 41(5):877–907. [PubMed: 14521200]
43. Noll DC, Nishimura DG, Macovski A. Homodyne detection in magnetic resonance imaging. IEEE Trans Med Imaging. 1991; 10(2):154–163. [PubMed: 18222812]
44. Roemer PB, Edelstein WA, Hayes CE, Souza SP, Mueller OM. The NMR phased array. Magn Reson Med. 1990; 16(2):192–225. [PubMed: 2266841]
45. Buxton RB, Frank LR, Wong EC, Siewert B, Warach S, Edelman RR. A general kinetic model for quantitative perfusion imaging with arterial spin labeling. Magn Reson Med. 1998; 40(3):383–396. [PubMed: 9727941]

NIH-PA Author Manuscript

NIH-PA Author Manuscript

NIH-PA Author Manuscript

46. Herscovitch P, Raichle ME. What is the correct value for the brain--blood partition coefficient for water? J Cereb Blood Flow Metab. 1985; 5(1):65–69. [PubMed: 3871783]
47. Bjornerud A, Johansson LO, Briley-Saebo K, Ahlstrom HK. Assessment of T1 and T2* effects in vivo and ex vivo using iron oxide nanoparticles in steady state--dependence on blood volume and water exchange. Magn Reson Med. 2002; 47(3):461–471. [PubMed: 11870832]
48. Schwarzbauer C, Morrissey SP, Deichmann R, Hillenbrand C, Syha J, Adolf H, Noth U, Haase A. Quantitative magnetic resonance imaging of capillary water permeability and regional blood volume with an intravascular MR contrast agent. Magn Reson Med. 1997; 37(5):769–777. [PubMed: 9126952]
49. Roberts DA, Rizi R, Lenkinski RE, Leigh JS Jr. Magnetic resonance imaging of the brain: blood partition coefficient for water: application to spin-tagging measurement of perfusion. J Magn Reson Imaging. 1996; 6(2):363–366. [PubMed: 9132103]
50. Bland, M. An Introduction to Medical Statistics. Oxford: Oxford University Press; 2000.
51. de Bazelaire CM, Duhamel GD, Rofsky NM, Alsop DC. MR imaging relaxation times of abdominal and pelvic tissues measured in vivo at 3.0 T: preliminary results. Radiology. 2004; 230(3):652–659. [PubMed: 14990831]
52. Valtin, H.; Schafer, J. Renal Function. Boston: Little, Brown and Company; 1995.
53. Constantinides CD, Atalar E, McVeigh ER. Signal-to-noise measurements in magnitude images from NMR phased arrays. Magn Reson Med. 1997; 38(5):852–857. [PubMed: 9358462]
54. Avasthi PS, Greene ER, Voyles WF. Noninvasive Doppler assessment of human postprandial renal blood flow and cardiac output. Am J Physiol. 1987; 252(6 Pt 2):F1167–F1174. [PubMed: 3591956]
55. Huber S, Bornstedt A, Schnackenburg B, Paetsch I, Fleck E, Nagel E. The impact of different positions and thoracial restrains on respiratory induced cardiac motion. J Cardiovasc Magn Reson. 2006; 8(3):483–488. [PubMed: 16755836]
56. Israel GM, Bosniak MA. How I do it: evaluating renal masses. Radiology. 2005; 236(2):441–450. [PubMed: 16040900]
57. Rofsky NM, Bosniak MA. MR imaging in the evaluation of small (< or =3.0 cm) renal masses. Magn Reson Imaging Clin N Am. 1997; 5(1):67–81. [PubMed: 8995125]
58. Scialpi M, Di Maggio A, Midiri M, Loperfido A, Angelelli G, Rotondo A. Small renal masses: assessment of lesion characterization and vascularity on dynamic contrast-enhanced MR imaging with fat suppression. AJR Am J Roentgenol. 2000; 175(3):751–757. [PubMed: 10954462]
59. Goldfarb JW, Prasad PV, Chen Q, Edelman RR. Simultaneous magnetic resonance gadolinium-enhanced 2D perfusion and 3D angiographic imaging. Magn Reson Imaging. 2003; 21(6):585–591. [PubMed: 12915188]
60. Huang AJ, Lee VS, Rusinek H. Functional renal MR imaging. Magn Reson Imaging Clin N Am. 2004; 12(3):469–486. vi. [PubMed: 15271366]
61. de Bazelaire C, Alsop DC, George D, Pedrosa I, Wang Y, Michaelson MD, Rofsky NM. Magnetic Resonance Imaging-Measured Blood Flow Change after Antiangiogenic Therapy with PTK787/ZK 222584 Correlates with Clinical Outcome in Metastatic Renal Cell Carcinoma. Clin Cancer Res. 2008; 14(17):5548–5554. [PubMed: 18765547]
62. Boss A, Martirosian P, Schraml C, Clasen S, Fenchel M, Anastasiadis A, Claussen CD, Pereira PL, Schick F. Morphological, contrast-enhanced and spin labeling perfusion imaging for monitoring of relapse after RF ablation of renal cell carcinomas. Eur Radiol. 2006; 16(6):1226–1236. [PubMed: 16752153]

NIH-PA Author Manuscript

NIH-PA Author Manuscript

NIH-PA Author Manuscript

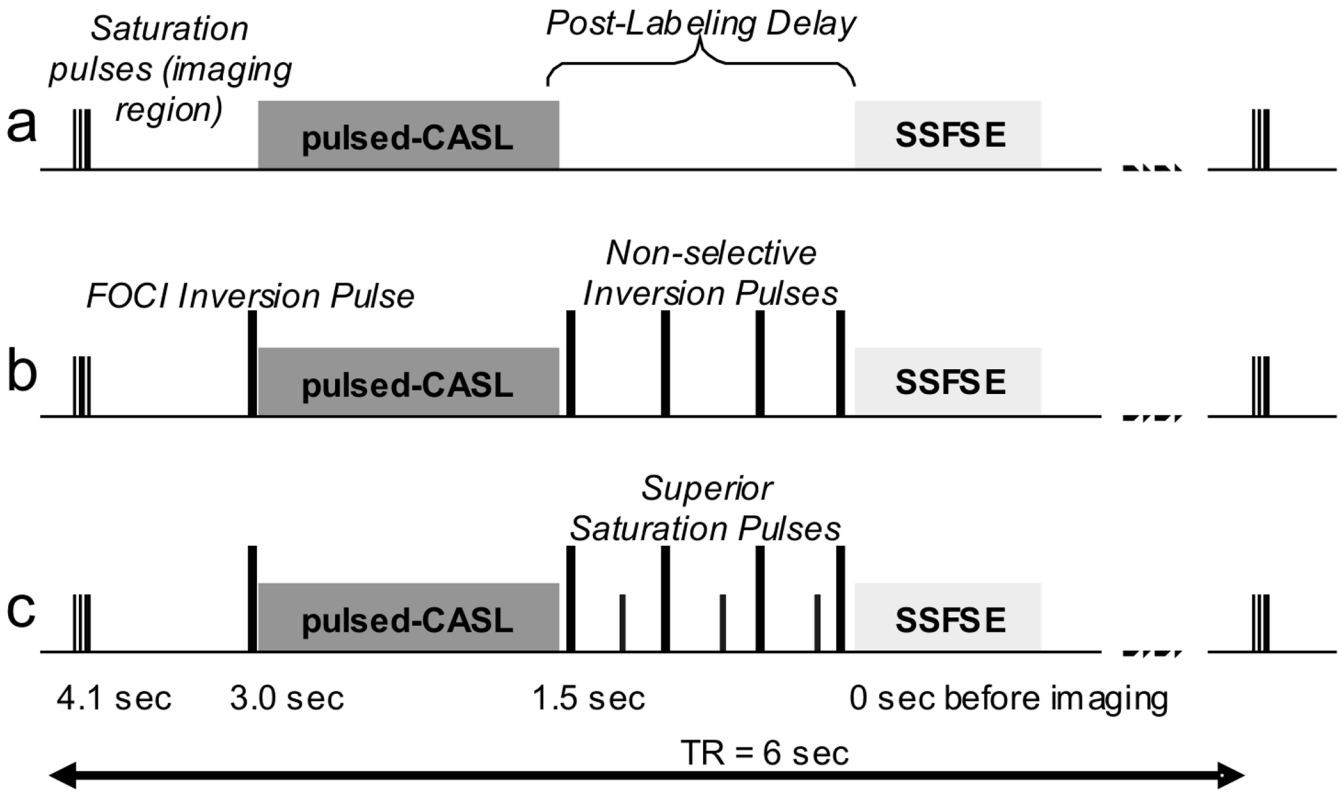

Figure 1.

The Pulse sequence diagram for ASL measurements. One 6-sec TR interval is shown, with time-before-imaging indicated: a) showing pulses for initial saturation of the imaging region (axially-orientated slab), pulsed-continuous labeling, the post-labeling delay, and a SSFSE image acquisition; b) the same with background suppression inversion pulses added (slab-selective FOCI pulse before labeling and the non-selective adiabatic inversion pulses after labeling); c) the same with pulses added for saturation of superior inflowing arterial blood.

NIH-PA Author Manuscript

NIH-PA Author Manuscript

NIH-PA Author Manuscript

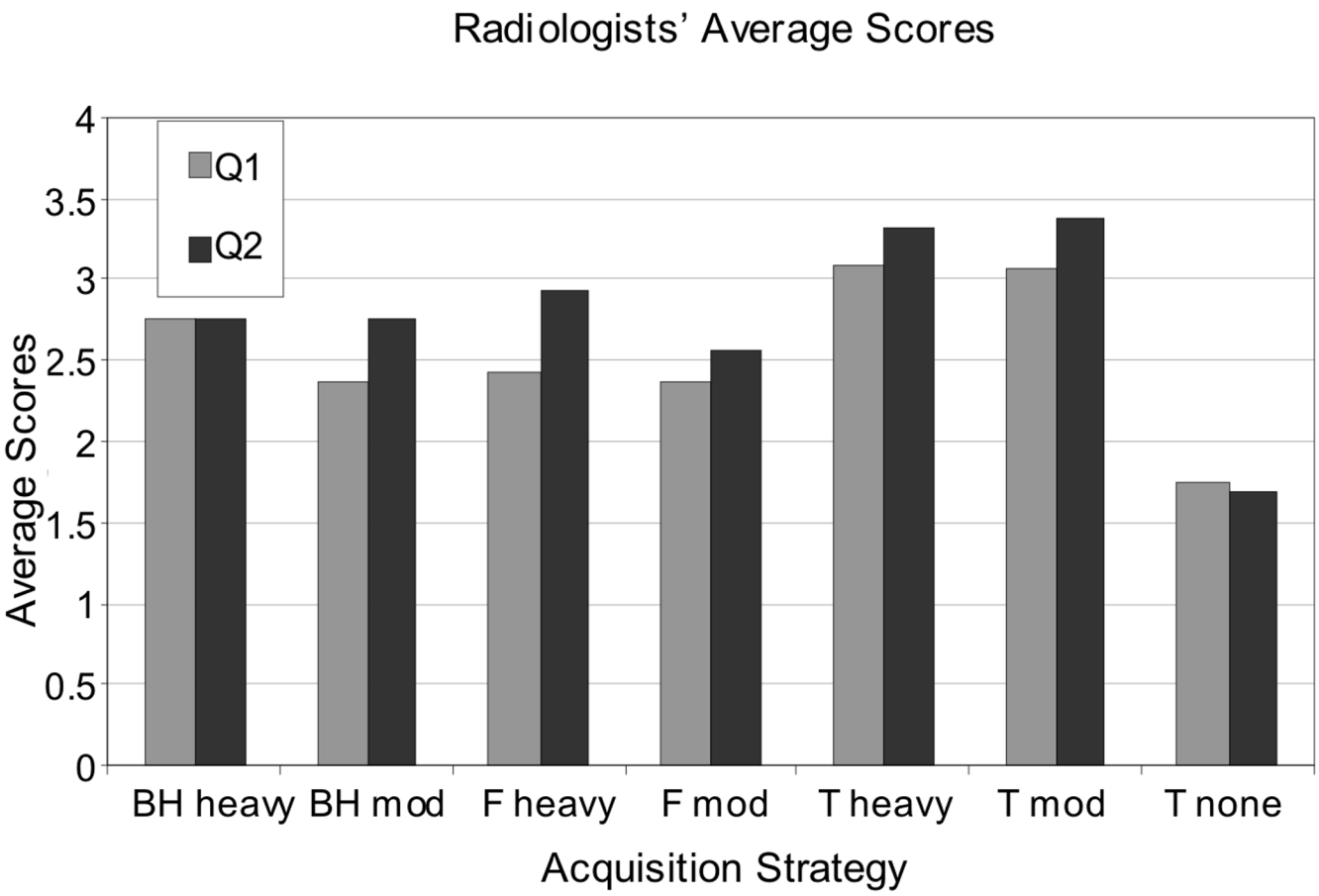

Figure 2.

Summary of image assessment by radiologists. Average scores over all subjects are shown for each combined background suppression and breathing strategy (pair of bars), and for assessment of questions "Q1" pertaining to the appearance of artifacts, and "Q2" pertaining to overall image quality; scores are averages of both radiologists' scores. (BH, F, and T refer to breathing strategy; 'heavy', 'mod', and 'none' refer to background suppression.) The most marked difference in scores is the low average scores for the scheme without any background suppression; a slight preference for timed breathing is also shown in its higher average scores.

NIH-PA Author Manuscript

NIH-PA Author Manuscript

NIH-PA Author Manuscript

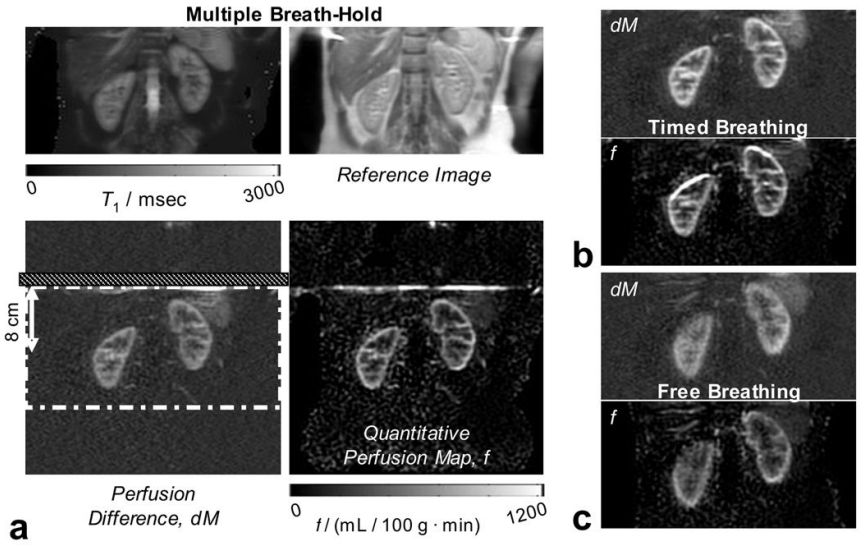

Figure 3.

Typical image quality in perfusion difference images and quantitative perfusion maps: a) the set of four images produced by the ASL experiment. Top left and right are the calculated T1 map and M_0-image from the reference images. Bottom-left and right are the perfusion difference image (dM) and the quantitative perfusion map (f). Regions of higher and lower perfusion correspond to the cortical and medullary tissue structures in the kidney as also identified in the reference images. The dot-dash white line in the dM image is the axially-oriented imaging region, which is saturated prior to labeling as part of background suppression. The labeling plane, located at the superior edge of the imaging region, and orientated axially, is identified by the hatched section. All images were acquired with heavy background suppression. Breathing strategies were: in a) multiple breath-hold; in b) timed; and in c) free breathing. Good image quality is achieved in all images however (c) illustrates a case where bulk motion during free breathing introduces additional blurring.

NIH-PA Author Manuscript

NIH-PA Author Manuscript

NIH-PA Author Manuscript

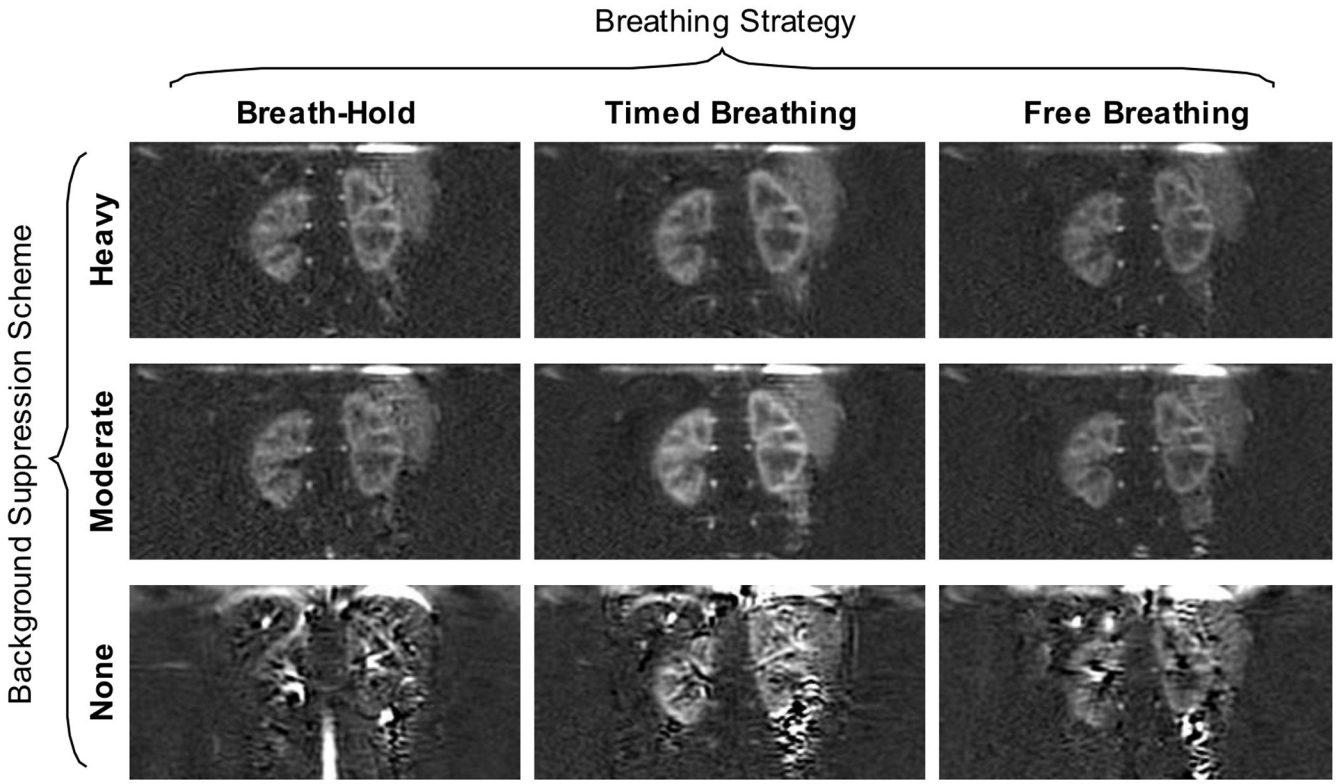

Figure 4.

Typical image quality in perfusion difference images for all imaging strategies. In the same volunteer, perfusion difference images are shown for each combination of background suppression and breathing strategy. Background suppression significantly improves image quality, removing artifacts from subtraction errors. In this volunteer, additional images without background suppression were acquired that were not repeated in all subjects for statistical analysis.

NIH-PA Author Manuscript

NIH-PA Author Manuscript

NIH-PA Author Manuscript

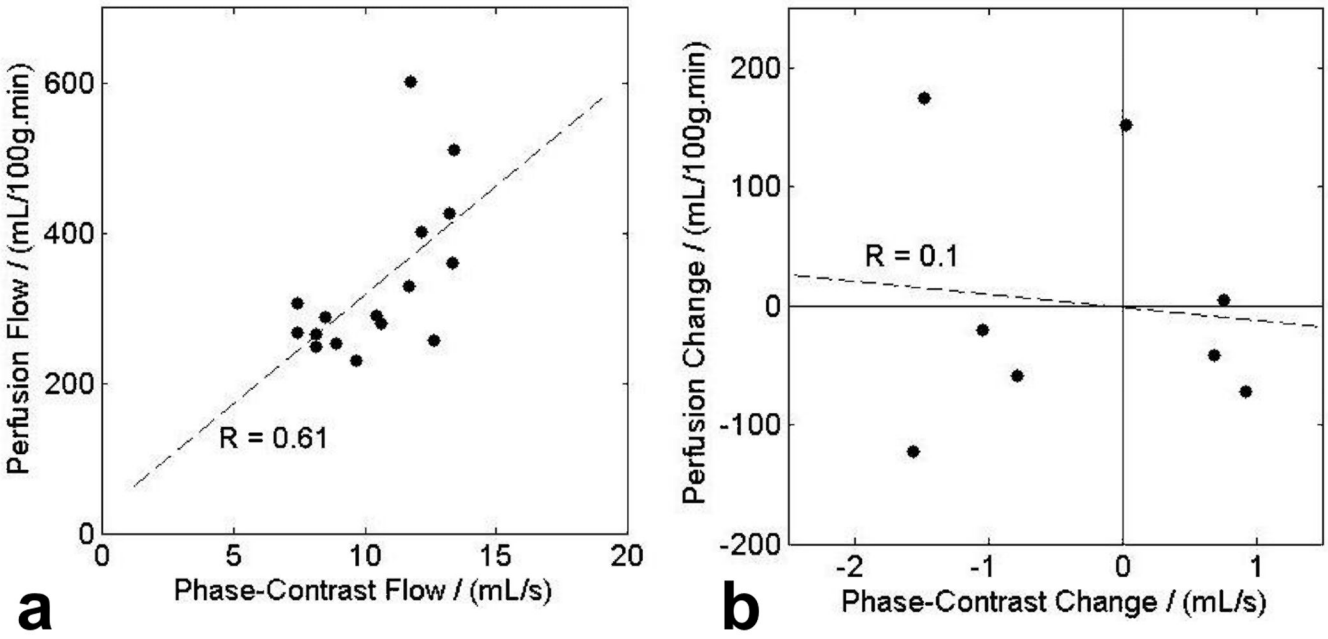

Figure 5.

a) Correlation between measured perfusion and measured total renal flow in both kidneys of four subjects at test and retest. There is a significant correlation (5% level), with correlation coefficient R = 0.61, slope 29 ± 10 (mL/100g.min)/(mL/s) and intercept 28 ± 111 (mL/100g.min)/(mL/s). b) Correlation between changes in flow measurements at test and retest; flow measured by perfusion and phase-contrast angiography. No significant correlation of changes is observed with R = 0.11 for 8 samples.

NIH-PA Author Manuscript

NIH-PA Author Manuscript

NIH-PA Author Manuscript

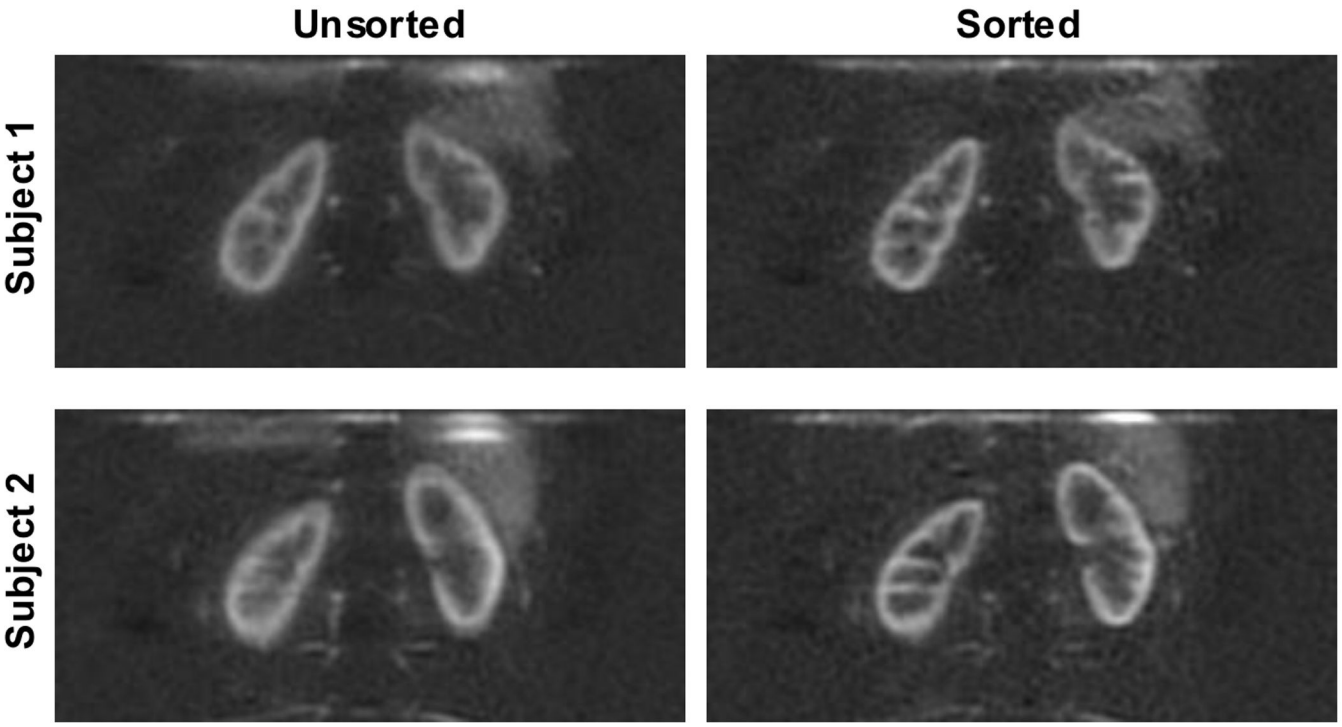

Figure 6.

Results from retrospective image sorting. In two subjects, perfusion difference images acquired during free breathing are shown (left), reconstructed from all 48 label-control pairs, and (right), after retrospectively sorting the images based on respiratory bellows position. During one quarter of the acquisition time, the subject was breathing deeply. The sorting strategy accepted the 50% of images closest to end-expiration. These images were acquired using the 'heavy' background suppression scheme.

NIH-PA Author Manuscript

NIH-PA Author Manuscript

NIH-PA Author Manuscript

Table 1

Test-retest repeatability, COV_F (standard deviation of perfusion measurement as a percentage of mean flow), for each combination of breathing and background suppression strategies

Between Session Repeatability			
	Breath-Hold	***Timed Breathing***	***Free Breathing***
Heavy Bckgrd Supp	7 % †	23 %	20 %
Moderate Bckgrd Supp	12 %	15 %	19 %
None		18 %	
In-Session Repeatability			
Heavy Bckgrd Supp		8 % *	

COV_F is significantly lower:

*(10% level, or better, for the *F*-test) compared to all other measurements except those for *Breath-Hold*,

†5% level, or better, compared to all other between-session measurements.

NIH-PA Author Manuscript NIH-PA Author Manuscript NIH-PA Author Manuscript

Table 2

Significance of perfusion measurement standard deviation (SD) differences in kidney regions of interest (ROI) with different respiratory and background suppression strategies. The *p*-value of a two-tailed *t*-test between ROI-SD values for pairs of strategies is tabulated. Comparisons are shown by column with common strategies in the column headings; abbreviations are: Timed breathing 'T', Breath-Hold 'BH', Free breathing 'F', Heavy BGS 'HBGS', Moderate BGS 'MBGS', no BGS 'no BGS', and '*versus*' denoted by **—**; e.g. the first entries represent *p*-values for ROIs in the cortex and medulla when comparing Timed breathing with Heavy BGS to Timed breathing with no BGS.

***versus* T-No BGS**			**Heavy BGS**			**Breath-Hold**		
	Cortex	**Medulla**		**Cortex**	**Medulla**		**Cortex**	**Medulla**
T-HBGS—	0.01	0.007	***BH— F***	0.54	0.53	***HBGS— MBGS***	0.7	0.87
T-MBGS—	0.0007	0.002	***T— BH***	0.35	0.69	**Timed Breathing**		
BH-HBGS—	0.0002	0.0002	***T— F***	0.19	0.37	***HBGS— MBGS***	0.61	0.87
BH-MBGS—	0.0007	0.0001	**Moderate BGS**			***HBGS— no BGS***	0.01	0.007
F-HBGS—	0.00007	0.00003	***BH— F***	0.45	0.53	***MBGS— no BGS***	0.0007	0.002
F-MBGS—	0.051	0.043	***T— BH***	0.90	0.67	**Free Breathing**		
			T— F	0.49	0.76	***HBGS— MBGS***	0.19	0.37

NIH-PA Author Manuscript

NIH-PA Author Manuscript

NIH-PA Author Manuscript

Table 3

Test-retest repeatability, COV_F, of perfusion calculations including retrospective sorting of ASL images based on respiratory position. Various sorting schemes are shown as well as a reference scheme which includes all acquired images.

Reference	Retrospective Sorting Scheme Criterion			
Timed Breathing	***First Set***	***End-Expiration***	***Median Position***	***Closest Together***
6.6 %	5.4 %	1.7 % *	6.8 %	2.5 % †

Significantly lower measurement variance when compared to all other schemes:

*1% level for the *F*-test,

†5% level

NIH-PA Author Manuscript

NIH-PA Author Manuscript

NIH-PA Author Manuscript

Table 4

Significance of perfusion measurement standard deviation (SD) differences in kidney regions of interest (ROI) with different retrospective sorting schemes. The *p*-value of a *t*-test between ROI-SD values for each sorting scheme compared to the reference scheme including all acquired images is tabulated.

Timed Breathing Reference vs Retrospective Sorting Schemes		
	Cortex	**Medulla**
First Set	0.33	0.81
End-Expiration	0.85	0.48
Median Position	0.78	0.80
Closest Together	0.85	0.68